Holocene history of ENSO variance and asymmetry in the eastern tropical Pacific

Matthieu Carré,[1]* Julian P. Sachs,[2] Sara Purca,[3] Andrew J. Schauer,[4] Pascale Braconnot,[5] Rommel Angeles Falcón,[6] Michèle Julien,[7] Danièle Lavallée[8]

[1]UM2-CNRS-IRD, Institut des Sciences de l'Evolution de Montpellier, UMR 5554, Pl. Eugène Bataillon, 34095 Montpellier, France. [2]University of Washington, School of Oceanography, Box 355351, Seattle, WA 98195, USA. [3]Instituto del Mar del Perú IMARPE, Esq. Gamarra y general Valle S/N, Callao, Perú. [4]University of Washington, Department of Earth and Space Sciences, Box 351310, Seattle, WA 98195, USA. [5]IPSL/Laboratoire des Sciences du Climat et de l'Environnement, unité mixte CEA-CNRS-UVSQ, Orme des merisiers, Bât. 712, 91191 Gif sur Yvette, France. [6]Ministerio de Cultura, Museo de sitio de Pachacamac, Lurín, Lima, Perú. [7]Archéologies et Sciences de l'Antiquité, UMR 7041, Maison René Ginouvès, 21 Allée de l'Université, 92023 Nanterre, France. [8]Archéologie des Amériques, UMR 8096, Maison René Ginouvès, 21 Allée de l'Université, 92023 Nanterre, France.

*Corresponding author. E-mail: matthieu.carre@univ-montp2.fr

Understanding the response of the El Niño-Southern Oscillation (ENSO) to global warming requires quantitative data on ENSO under different climate regimes. Here we present a reconstruction of ENSO in the eastern tropical Pacific spanning the last 10 thousand years (ka) derived from oxygen isotopes in fossil mollusk shells from Peru. We find that ENSO variance was close to the modern level in the early Holocene and severely damped ~4-5 ka. In addition, ENSO variability was skewed toward cold events along coastal Peru 6.7-7.5 ka owing to a shift of warm anomalies toward the Central Pacific. The modern ENSO regime was established ~3-4.5 ka. We conclude that ENSO was sensitive to changes in climate boundary conditions during the Holocene, including, but not limited to insolation.

The El Niño-Southern Oscillation (ENSO) represents the largest natural perturbation to the global climate on an inter-annual time scale, impacting ecosystems and economies globally. Predicting how the amplitude and spatial pattern of ENSO will change in response to evolving radiative forcing from the buildup of greenhouse gases in the atmosphere is a scientific challenge (*1*) that requires knowledge of the character of ENSO under a range of climate boundary conditions as observed during the Holocene epoch.

A central paradigm of ENSO-mean state studies for the last decade has been that changes in insolation resulting from cyclical changes in Earth's orbital geometry exert a strong control on ENSO (*2–4*). This hypothesis was recently called into question by a series of coral oxygen isotope (δ18O) records from the Line Islands in the central Pacific showing large variability in the amplitude of ENSO variance over the last 7 kyr, but no significant difference between the middle Holocene and the last millennium (*5*). Furthermore, no reconstructions of ENSO have yet been able to document changes in the spatial pattern of ENSO that are now recognized to account for an important component of its global teleconnections (*6*). Here we use a technique based on oxygen isotope variations in fossil mollusk shells from the coast of Peru (*7*) to quantify changes in the amplitude and spatial pattern of ENSO through the Holocene.

We reconstructed the distribution of ENSO-related sea surface temperature (SST) anomalies in the eastern tropical Pacific from monthly records of δ18O values in fossil *Mesodesma donacium* shells on the coast of Peru. *M. donacium* is a fast growing aragonitic bivalve that inhabits the surf zone of sandy beaches. Well-preserved shells were collected from radiocarbon-dated intervals at 7 coastal archaeological sites [e.g., (*8*)] between 11.7 °S and 18.1 °S (Fig. 1, fig. S1, and table S1). *M. donacium* has been gathered and consumed by fishermen for more than 10,000 years (*9*), resulting in anthropogenic shell mounds up to 10 m in height along the Peruvian coastal desert (figs. S2 to S8). Shells were generally perfectly preserved owing to extremely arid conditions, ensuring the fidelity of δ18O values [e.g., (*8*), figs. S9 to S10]. Previous calibration work has demonstrated that *M. donacium* shells faithfully record 1-4 years of SST variability with ~1 month resolution (Fig. 1C), yielding quantitative estimates of the seasonal SST range (ΔT) in the coastal water (*10*). By analyzing a random sample of shells from a single depth interval that encompasses several decades or centuries of accumulation, the mean, variance, and skewness of coastal ΔT is obtained, as validated with modern specimens (*7*). A rigorous evaluation of the standard errors of the mean, variance, and skewness of coastal ΔT was conducted with a series of pseudo-proxy Monte Carlo simulations that took into consideration the uncertainties associated with isotopic analyses, sampling within climate variability, mesoscale spatial variability, and shell growth, enabling the statistical significance of results to be ascertained (*11*).

Peruvian surf clams share similarities with corals as paleoclimate proxies in that the seasonality of SST can be resolved (*5*), and with individual foraminifera (*12*), since a sample of several specimens is required to statistically extract ENSO characteristics. *M. donacium* shells record ENSO variance resulting from La Niña anomalies and moderate El Niño anomalies, but importantly, do not record extreme El Niño events. When coastal Peru SSTs warm dramatically (maximum anomaly of 7.7°C in January 1998 in Callao) mass mortality of *M. donacium* occurs. Nevertheless, the distribution of ΔT from a sample of modern shells, though truncated, accurately captures the positively skewed distribution of ENSO in the eastern Pacific (*7*). Our composite Holocene record from 180 mollusk shells and 7 archaeological sites thus yields a quantitative reconstruction of mean annual SST, mean ΔT, as well as ENSO variance and skewness for coastal Peru. Because the variance of coastal Peruvian ΔT is highly correlated with the variance of SST anomalies in the Niño1+2 region (R=0.85), var(ΔT) in Peru can be used as a reliable indicator of ENSO variance in the eastern tropical Pacific (*7*).

Mean annual SST was significantly lower than today 4.5-9.6 ka, especially in southern Peru, where SSTs were ~3°C cooler (Fig. 2A). These cooler conditions imply an increase in the intensity of coastal upwelling (*13*, *14*). Although highly variable, the seasonal range of SST (ΔT) was significantly reduced compared to the late 20th century during most of the Holocene, with reductions up to ~30% (equivalent to ~1.1°C) 0.5, 4.7, 8.5 and 9.5 ka (Fig. 2B). Furthermore, ENSO variability, as derived from the variance of ΔT, was higher in the late 20th century than at any other sampled interval of the Holocene, even excluding the influence of the 1982-83 and 1997-98 extreme El Niño events (Fig.

3A). The lowest ENSO variance in the eastern tropical Pacific occurred at ~4.7ka (55% reduction, 82% confidence level) (Fig. 3A).

A Holocene minimum in ENSO variance 4-5 ka is supported by a sedimentary record of $\delta^{18}O$ values in individual planktonic foraminifera from near the Galápagos that also indicates highly variable conditions throughout the Holocene, interrupted by a period of low foraminiferal $\delta^{18}O$ variance 4-5 ka (Fig. 3C) (12). In addition to inter-annual SST variability, however, the variance of foraminiferal $\delta^{18}O$ in marine sediments is influenced by decadal variability, and changing precession-driven seasonality. In the central Pacific, coral $\delta^{18}O$ records indicate lower than modern ENSO variance during the Holocene, with large variations before 6 ka and after 3 ka, and a minimum in ENSO variance 3-5 ka (5). Although the latter result is not statistically significant in light of the full data set (5), its robustness is now increased by the consistent variance reduction observed in our Peru mollusk record and the foraminiferal record from the Galapagos (12). Further support for low ENSO variance in the 4-5 ka time period comes from a 175-year coral $\delta^{18}O$ record from Christmas Island, which indicated a 79% reduction of ENSO variance in the central Pacific at ~4.3 ka (15). A network of evidence thus supports the occurrence of a substantial multi-centennial reduction of ENSO variance 4-5 ka across the Niño3.4 and Niño1+2 domains.

ENSO variance recorded by Peru mollusks 6-10 ka was variable but not statistically different from the Late Holocene. Our reconstruction combined with early Holocene dates of flood deposits in coastal Peru (16–18) challenge the hypothesis of little or no ENSO variance before ~5ka (19–21), a conclusion based largely on the analysis of clastic sediments in Lake Pallcacocha (19, 20). However, clastic sediments in high Andean Lakes have recently been re-interpreted in terms of soil erosion from mountain glacier activity rather than from rainfall events associated with ENSO (22). The only reliable marine evidence for inactive ENSO in the early to middle Holocene is provided by corals from Papua New Guinea (23). Apparent disagreements between ENSO records from the Western and Eastern Pacific may in fact be indicative of changes in the spatial pattern of ENSO.

Two spatial modes of ENSO variability have been described, defined by maximum SST anomalies localized in the central Pacific (CP) or eastern Pacific (EP) (24, 25). The EP mode tends to produce strong El Niño warming events in the East and moderate La Niña events. This well-known asymmetry between El Niño and La Niña events results in a positively skewed distribution of SST anomalies (Fig. 1A). The CP mode tends to produce moderate El Niño events centered in the central Pacific and strong La Niña events, resulting in a negatively skewed distribution of SST anomalies in Peru as shown by instrumental data (24–26). The skewness of ENSO anomalies in fossil shell samples thus tracks past changes in the dominant spatial pattern of ENSO variability (8). Skewness values in the fossil record are positive and similar to modern conditions during most of the Holocene, except for the period 6.7-7.5 ka when a significant shift (95% confidence level) toward negative skewness occurred (Fig. 3E). This result implies that the SST variability in the eastern Pacific at that time was driven by cold anomalies, and that warm anomalies in the Niño1+2 region were less frequent and/or intense. A possible explanation for this pattern may be a predominantly CP mode of ENSO 6.7-7.5 ka.

This hypothesis is supported by a record of flood events from the Peru margin (27) (Fig. 3B). High lithic concentrations (exceeding 4σ of the signal) in a sediment core from the continental shelf off central Peru record coastal floods due to extreme El Niño events typical of the EP mode (28). By indicating extreme El Niño events, this proxy thus fills the gap of ENSO variance that is not recorded by Peruvian mollusk shells (supplementary text). That record clearly shows the occurrence of 8 large flood events prior to 8 ka and 14 after 4 ka (Fig. 3B), which is also consistent with earlier studies of flood-related debris flow deposits in Peru (16, 17, 29). This is in agreement with the mollusk $\delta^{18}O$ data

indicating significant ENSO activity dominated by the EP mode before 8 ka and after 4 ka. From 6.7-7.5 ka, on the other hand, the complete absence of flood events contrasts with the significant though weaker ENSO variance reconstructed from mollusk shells. This apparent disagreement can be most simply explained by a predominance of the CP mode of ENSO at that time, as implied by the negative skewness of the ΔT distribution (Fig. 3E). CP El Niño events have a different teleconnection pattern and do not generate rainfall anomalies on the Peruvian coast.

A central question in climate science is the extent to which changes in the climatic mean state influence ENSO variability. Long unforced climate simulations exhibit multidecadal internally-generated changes in ENSO behavior (30). Our data indicate that changes in the character of ENSO during the Holocene persisted for centuries, exceeding the time scale of model-generated internal variability. We therefore surmise that ENSO is sensitive to external forcing. Climate models forced by 6 ka and 9.5 ka insolation produce a cooling and reduced ΔT in the eastern Pacific, along with reduced ENSO variance (3, 4). The simulated impact of insolation is consistent with the mean annual and seasonal range of SST derived from Peru mollusks, but not for ENSO variance, which the mollusks indicate was high in the early Holocene. Climate simulations have demonstrated that a freshwater flux into the North Atlantic could offset the impact of insolation on ENSO in the early Holocene (31). Our data support this scenario and imply that any tendency toward lower ENSO variance during the mid-Holocene insolation regime may have been counteracted 6.7-10 ka by the influence of melting ice-sheets (31). While the low ENSO activity 4-5 ka is consistent with precessional forcing, the shift of ENSO asymmetry 6.7-7.5 ka points to factors within the climate system influencing changes in the spatial pattern of ENSO.

References and Notes

1. A. Santoso, S. McGregor, F. F. Jin, W. Cai, M. H. England, S. I. An, M. J. McPhaden, E. Guilyardi, Late-twentieth-century emergence of the El Niño propagation asymmetry and future projections. *Nature* **504**, 126–130 (2013). Medline doi:10.1038/nature12683
2. A. C. Clement, R. Seager, M. A. Cane, Orbital controls on the El Niño/Southern Oscillation and the tropical climate. *Paleoceanography* **14**, 441–456 (1999). doi:10.1029/1999PA900013
3. W. Zheng, P. Braconnot, E. Guilyardi, U. Merkel, Y. Yu, ENSO at 6ka and 21ka from ocean–atmosphere coupled model simulations. *Clim. Dyn.* **30**, 745–762 (2008). doi:10.1007/s00382-007-0320-3
4. Y. Luan, P. Braconnot, Y. Yu, W. Zheng, O. Marti, Early and mid-Holocene climate in the tropical Pacific: Seasonal cycle and interannual variability induced by insolation changes. *Clim. Past* **8**, 1093–1108 (2012). doi:10.5194/cp-8-1093-2012
5. K. M. Cobb, N. Westphal, H. R. Sayani, J. T. Watson, E. Di Lorenzo, H. Cheng, R. L. Edwards, C. D. Charles, Highly variable El Niño-Southern Oscillation throughout the Holocene. *Science* **339**, 67–70 (2013). Medline doi:10.1126/science.1228246
6. T. Lee, M. J. McPhaden, *Geophys. Res. Lett.* **37**, L14603 (2010).
7. M. Carré, J. P. Sachs, A. J. Schauer, W. E. Rodríguez, F. C. Ramos, *Palaeogeogr. Palaeoclimatol. Palaeoecol.* **371**, 45 (2013). doi:10.1016/j.palaeo.2012.12.014
8. Materials and methods are available as supplementary materials on *Science* Online.
9. D. H. Sandweiss, H. McInnis, R. L. Burger, A. Cano, B. Ojeda, R. Paredes, M. C. Sandweiss, M. D. Glascock, Quebrada jaguay: Early south american maritime adaptations. *Science* **281**, 1830–1832 (1998). Medline doi:10.1126/science.281.5384.1830
10. M. Carré, I. Bentaleb, D. Blamart, N. Ogle, F. Cardenas, S. Zevallos, R. M. Kalin, L. Ortlieb, M. Fontugne, Stable isotopes and sclerochronology of the bivalve Mesodesma donacium: Potential application to Peruvian paleoceanographic reconstructions. *Palaeogeogr. Palaeoclimatol. Palaeoecol.* **228**, 4–25 (2005). doi:10.1016/j.palaeo.2005.03.045
11. M. Carré, J. P. Sachs, J. M. Wallace, C. Favier, Exploring errors in paleoclimate proxy reconstructions using Monte Carlo simulations: Paleotemperature from mollusk and coral geochemistry. *Clim. Past* **8**, 433–

450 (2012). doi:10.5194/cp-8-433-2012

12. A. Koutavas, S. Joanides, El Niño-Southern Oscillation extrema in the Holocene and Last Glacial Maximum. *Paleoceanography* **27**, PA4208 (2012). doi:10.1029/2012PA002378

13. M. Carré, M. Azzoug, I. Bentaleb, B. M. Chase, M. Fontugne, D. Jackson, M.-P. Ledru, A. Maldonado, J. P. Sachs, A. J. Schauer, Mid-Holocene mean climate in the south eastern Pacific and its influence on South America. *Quat. Int.* **253**, 55–66 (2012). doi:10.1016/j.quaint.2011.02.004

14. J. Sadler, M. Carré, M. Azzoug, A. J. Schauer, J. Ledesma, F. Cardenas, B. M. Chase, I. Bentaleb, S. D. Muller, M. Mandeng, E. J. Rohling, J. P. Sachs, Reconstructing past upwelling intensity and the seasonal dynamics of primary productivity along the Peruvian coastline from mollusk shell stable isotopes. *Geochem. Geophys. Geosyst.* **13**, Q01015 (2012). doi:10.1029/2011GC003595

15. H. V. McGregor, M. J. Fischer, M. K. Gagan, D. Fink, S. J. Phipps, H. Wong, C. D. Woodroffe, A weak El Niño/Southern Oscillation with delayed seasonal growth around 4,300 years ago. *Nat. Geosci.* **6**, 949–953 (2013). doi:10.1038/ngeo1936

16. M. Fontugne, P. Usselmann, D. Lavallée, M. Julien, C. Hatté, El Niño Variability in the Coastal Desert of Southern Peru during the Mid-Holocene. *Quat. Res.* **52**, 171–179 (1999). doi:10.1006/qres.1999.2059

17. D. K. Keefer, M. E. Moseley, S. D. deFrance, A 38 000-year record of floods and debris flows in the Ilo region of southern Peru and its relation to El Niño events and great earthquakes. *Palaeogeogr. Palaeoclimatol. Palaeoecol.* **194**, 41–77 (2003). doi:10.1016/S0031-0182(03)00271-2

18. D. H. Sandweiss *et al*., in *Climate Change and Cultural Dynamics: A Global Perspective on Mid-Holocene Transitions* D. G. Anderson, K. A. Maasch, D. H. Sandweiss, Eds. (Academic Press, Elsevier, 2007) pp. 25-50.

19. D. T. Rodbell, G. O. Seltzer, D. M. Anderson, M. B. Abbott, D. B. Enfield, J. H. Newman, An approximately 15,000-year record of El Nino-driven alluviation in southwestern ecuador. *Science* **283**, 516–520 (1999). Medline doi:10.1126/science.283.5401.516

20. C. M. Moy, G. O. Seltzer, D. T. Rodbell, D. M. Anderson, Variability of El Niño/Southern Oscillation activity at millennial timescales during the Holocene epoch. *Nature* **420**, 162–165 (2002). Medline doi:10.1038/nature01194

21. J. L. Conroy, J. T. Overpeck, J. E. Cole, T. M. Shanahan, M. Steinitz-Kannan, Holocene changes in eastern tropical Pacific climate inferred from a Galápagos lake sediment record. *Quat. Sci. Rev.* **27**, 1166–1180 (2008). doi:10.1016/j.quascirev.2008.02.015

22. D. T. Rodbell, G. O. Seltzer, B. G. Mark, J. A. Smith, M. B. Abbott, Clastic sediment flux to tropical Andean lakes: Records of glaciation and soil erosion. *Quat. Sci. Rev.* **27**, 1612–1626 (2008). doi:10.1016/j.quascirev.2008.06.004

23. A. W. Tudhope, C. P. Chilcott, M. T. McCulloch, E. R. Cook, J. Chappell, R. M. Ellam, D. W. Lea, J. M. Lough, G. B. Shimmield, Variability in the El Niño-Southern Oscillation through a glacial-interglacial cycle. *Science* **291**, 1511–1517 (2001). Medline doi:10.1126/science.1057969

24. H.-Y. Kao, J.-Y. Yu, Contrasting Eastern-Pacific and Central-Pacific Types of ENSO. *J. Clim.* **22**, 615–632 (2009). doi:10.1175/2008JCLI2309.1

25. S. I. An, F. F. Jin, Nonlinearity and Asymmetry of ENSO. *J. Clim.* **17**, 2399–2412 (2004). doi:10.1175/1520-0442(2004)017<2399:NAAOE>2.0.CO;2

26. B. Dewitte, J. Vazquez-Cuervo, K. Goubanova, S. Illig, K. Takahashi, G. Cambon, S. Purca, D. Correa, D. Gutierrez, A. Sifeddine, L. Ortlieb, Change in El Niño flavours over 1958–2008: Implications for the long-term trend of the upwelling off Peru. *Deep Sea Res. Part II Top. Stud. Oceanogr.* **77-80**, 143–156 (2012). doi:10.1016/j.dsr2.2012.04.011

27. B. Rein, A. Lückge, L. Reinhardt, F. Sirocko, A. Wolf, W.-C. Dullo, El Niño variability off Peru during the last 20,000 years. *Paleoceanography* **20**, n/a (2005). 10.1029/2004PA001099 doi:10.1029/2004PA001099

28. B. Rein, How do the 1982/83 and 1997/98 El Niños rank in a geological record from Peru? *Quat. Int.* **161**, 56–66 (2007). doi:10.1016/j.quaint.2006.10.023

29. L. E. Wells, Holocene history of the El Niño phenomenon as recorded in flood sediments of northern coastal Peru. *Geology* **18**, 1134 (1990). doi:10.1130/0091-7613(1990)018<1134:HHOTEN>2.3.CO;2

30. A. T. Wittenberg, Are historical records sufficient to constrain ENSO simulations? *Geophys. Res. Lett.* **36**, L12702 (2009). doi:10.1029/2009GL038710

31. P. Braconnot, Y. Luan, S. Brewer, W. Zheng, Impact of Earth's orbit and freshwater fluxes on Holocene climate mean seasonal cycle and ENSO characteristics. *Clim. Dyn.* **38**, 1081–1092 (2012). doi:10.1007/s00382-011-1029-x

32. K. Takahashi, A. Montecinos, K. Goubanova, B. Dewitte, ENSO regimes: Reinterpreting the canonical and Modoki El Niño. *Geophys. Res. Lett.* **38**, L10704 (2011). doi:10.1029/2011GL047364

33. R. W. Reynolds, N. A. Rayner, T. M. Smith, D. C. Stokes, W. Wang, An Improved In Situ and Satellite SST Analysis for Climate. *J. Clim.* **15**, 1609–1625 (2002). doi:10.1175/1520-0442(2002)015<1609:AIISAS>2.0.CO;2

34. F. Engel, *Southwest. J. Anthropol.* **13**, 54 (1957).

35. F. Engel, Les amas de coquillages de la côte péruvienne (Ancón-Río Ica). *J. Soc. Am.* **44**, 39–47 (1955). doi:10.3406/jsa.1955.2594

36. J. H. Rowe, Archaeological Explorations in Southern Peru, 1954-1955. *Am. Antiq.* **22**, 135 (1956). doi:10.2307/276816

37. D. Lavallée *et al*., *Chungara. Revista de Antropología Chilena* **43**, 333 (2011).

38. D. Lavallée, M. Julien, Prehistoria de la Costa Extremo-Sur del Perú. Los Pescadores Arcaicos de la Quebrada de los Burros (10000 –7000 a.P.) (Travaux de l'Institut Français d'Etudes Andines, Lima, 2012), pp. 478.

39. L. Ortlieb, G. Vargas, J.-F. Saliège, Marine radiocarbon reservoir effect along the northern Chile–southern Peru coast (14–24°S) throughout the Holocene. *Quat. Res.* **75**, 91–103 (2011). doi:10.1016/j.yqres.2010.07.018

40. B. Schöne, D. Bentley, *Nautilus* **116**, 25 (2002).

41. C. P. Glover, S. M. Kidwell, Influence of Organic Matrix on the Post-Mortem Destruction of Molluscan Shells. *J. Geol.* **101**, 729–747 (1993). doi:10.1086/648271

42. T. S. Tobin, A. J. Schauer, E. Lewarch, Alteration of micromilled carbonate δ18O during Kiel Device analysis. *Rapid Commun. Mass Spectrom.* **25**, 2149–2152 (2011). Medline doi:10.1002/rcm.5093

43. K. Lambeck, J. Chappell, Sea level change through the last glacial cycle. *Science* **292**, 679–686 (2001). Medline doi:10.1126/science.1059549

44. J.-C. Duplessy, L. Labeyrie, C. Waelbroeck, Constraints on the ocean oxygen isotopic enrichment between the Last Glacial Maximum and the Holocene: Paleoceanographic implications. *Quat. Sci. Rev.* **21**, 315–330 (2002). doi:10.1016/S0277-3791(01)00107-X

45. K. M. Cobb, C. D. Charles, H. Cheng, R. L. Edwards, El Niño/Southern Oscillation and tropical Pacific climate during the last millennium. *Nature* **424**, 271–276 (2003). Medline doi:10.1038/nature01779

46. D. H. Sandweiss, in *Case Studies in Environmental Archaeology* E. J. Reitz, L. A. Newsom, S. J. Scudder, Eds. (Plenum Press, New York, 1996).

47. D. H. Sandweiss, K. A. Maasch, R. L. Burger, J. B. Richardson III, H. B. Rollins, A. Clement, Variation in Holocene El Niño frequencies: Climate records and cultural consequences in ancient Peru. *Geology* **29**, 603 (2001). doi:10.1130/0091-7613(2001)029<0603:VIHENO>2.0.CO;2

48. D. H. Sandweiss, Terminal Pleistocene through Mid-Holocene archaeological sites as paleoclimatic archives for the Peruvian coast. *Palaeogeogr. Palaeoclimatol. Palaeoecol.* **194**, 23–40 (2003). doi:10.1016/S0031-0182(03)00270-0

49. T. J. De Vries, L. E. Wells, Thermally-anomalous Holocene molluscan assemblages from coastal Peru: Evidence for paleographic, not climatic change. *Palaeogeogr. Palaeoclimatol. Palaeoecol.* **81**, 11–32 (1990). doi:10.1016/0031-0182(90)90037-8

50. C. Perrier, C. Hillaire-Marcel, L. Ortlieb, Paléogéographie littorale et enregistrement isotopique (C, O) d'événements de type El Niño par les mollusques holocènes et récents du nord-ouest péruvien. *Geogr. Phys. Quat.* **48**, 23 (1994). doi:10.7202/032970ar

51. T. J. De Vries *et al*., Determining the Early History of El Nio. *Science* **276**, 965–967 (1997). doi:10.1126/science.276.5314.965

52. C. F. T. Andrus, D. E. Crowe, D. H. Sandweiss, E. J. Reitz, C. S. Romanek, Otolith delta 18O record of mid-Holocene sea surface temperatures in Peru. *Science* **295**, 1508–1511 (2002). Medline doi:10.1126/science.1062004

53. P. Béarez, T. J. DeVries, L. Ortlieb, Comment on "Otolith delta18O record of mid-Holocene sea surface temperatures in Peru". *Science* **299**, 203a (2003). Medline doi:10.1126/science.1076173

54. G. Vargas, J. Rutllant, L. Ortlieb, ENSO tropical–extratropical climate teleconnections and mechanisms for Holocene debris flows along the hyperarid coast of western South America (17°–24°S). *Earth Planet. Sci. Lett.* **249**, 467–483 (2006). doi:10.1016/j.epsl.2006.07.022

55. B. Mächtle, I. Unkel, B. Eitel, B. Kromer, S. Schiegl, Molluscs as evidence

for a late Pleistocene and early Holocene humid period in the southern coastal desert of Peru (14.5°S). *Quat. Res.* **73**, 39–47 (2010). doi:10.1016/j.yqres.2009.05.007

56. S. Rome-Gaspaldy, J. Ronchail, *Bull. Inst. Fr. Etudes Andines* **27**, 675 (1998).

Supplementary Materials
www.sciencemag.org/content/science.1252220/DC1
Materials and Methods
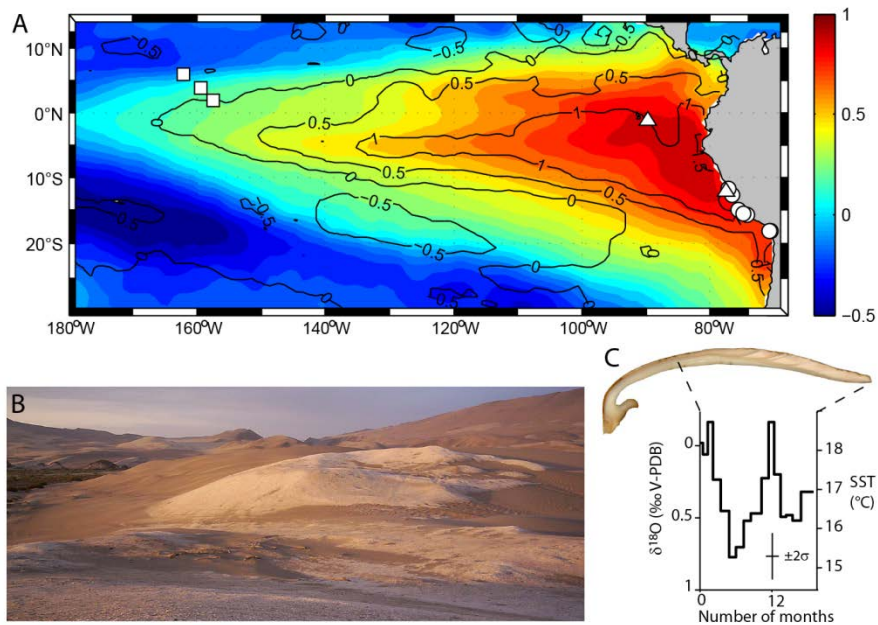Supplementary Text
Figs. S1 to S11
Tables S1 to S3
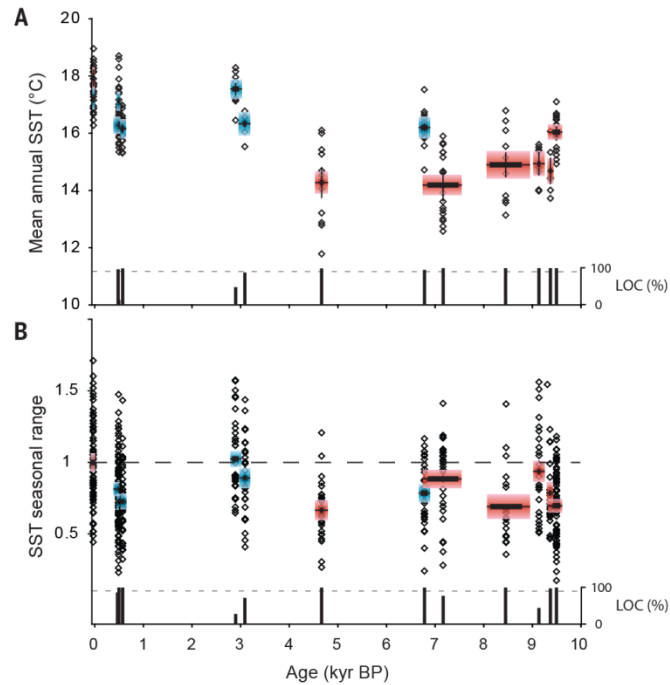References (*34–56*)
Data Tables S1 to S3
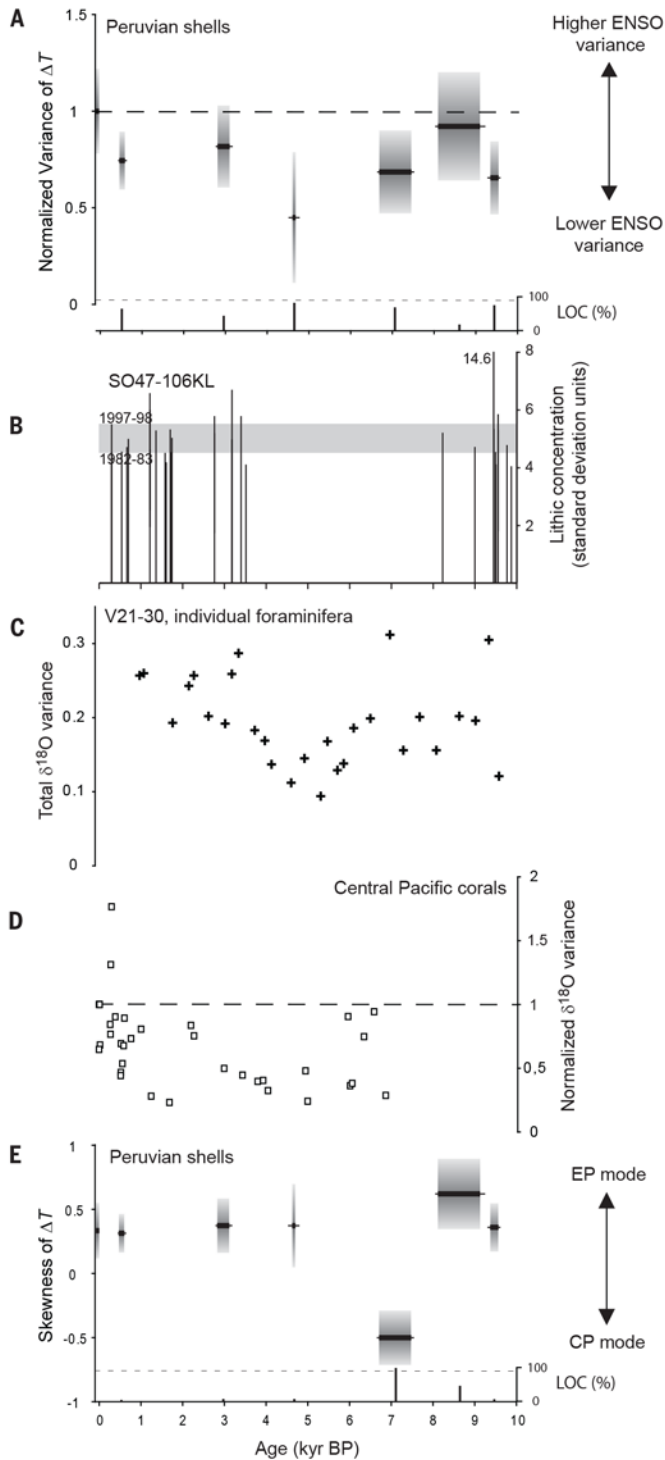
Fig. 1. (**A**) map of the central and eastern tropical Pacific indicating the location of shell middens (circles), sediment cores (triangles), and coral records (squares) discussed in the text. The skewness of monthly SST anomalies for the 1950-2010 period is represented by isolines, and the eastern Pacific pattern of ENSO as defined in (*32*) is represented by color shades. For this analysis the NOAA NCEP EMC CMB GLOBAL Reyn_SmithOIv2product that merges satellite and station data (*33*) was employed. (**B**) Picture of the northern part of the Ica-IS2 archaeological shell midden in the lower Ica valley, Peru (*8*). (**C**) Illustrative example of a *Mesodesma donacium* cross section and its associated monthly isotopic record converted to SST (shell ICA-1, *8*).

Fig. 2. Holocene reconstruction of mean annual SST and seasonal SST range from fossil mollusk δ^{18}O values on the Peru coast. (**A**) Mean SST values obtained from individual shells (open diamonds). For each shell midden, the average SST was represented over the occupation timespan (thick horizontal line, prolonged by a thin line for the 1σ calibration interval). The standard error (±1σ) of reconstructed SSTs is represented by blue bars for the central coast and red bars for the southern coast of Peru (fig. S1). A second error bar (±1σ) incorporates any potential systematic error introduced by calibration of the mollusk δ^{18}O SST proxy plus uncertainty in the correction for ice volume effects on ocean δ^{18}O (*8, 11*). The level of confidence (LOC) that reconstructed values of mean annual SST are significantly different from modern SSTs (student *t* test) is indicated by black bars in the lower portion of both panels, with the dotted line indicating the 90% LOC. (**B**) Seasonal ranges of *M. donacium* shell δ^{18}O normalized to the modern mean value. Individual shells record one to eight successive ΔT values (open diamonds) (*8*). For each shell midden, average values and standard errors were represented as in (A). The Horizontal dashed line represents modern conditions. LOC are indicated as in (A).

Fig. 3. Holocene records of ENSO from the eastern and central Tropical Pacific Ocean. (**A**) Normalized variance of ΔT values in mollusk shell samples (this study) indicating ENSO variance in the Niño1+2 region, with ±1σ standard errors (grey boxes). LOC are indicated as in Fig. 2A. (**B**) Extreme flood events in coastal Peru inferred from lithic concentrations in excess of 4σ of the detrended signal in the SO147-106KL sediment core (*26*) (Supplementary online text). The level for the very stong El Niño events in 1982-83 and 1997-98 is indicated by grey shading for comparison. (**C**) δ18O variance of individual *G. ruber* planktonic foraminifera in core V21-30 from near the Galápagos (*12*). (**D**) ENSO variance inferred from δ18O values of fossil corals from the Northern Line Islands of Palmyra, Fanning, and Christmas (*5*), normalized by the modern variance at each location (*8*). (**E**) Skewness of ΔT in *M. donacium* shell samples (this study) with standard errors (±1σ), indicating the relative contribution of CP and EP ENSO modes. LOC is shown as in Fig. 2A.